# Visualization of microstructural mechanisms in nanocrystalline ferrite during grinding

P. Grützmacher [a], C. Gachot [a], S.J. Eder [a,b,*]

[a] Institute for Engineering Design and Product Development, TU Wien, Getreidemarkt 9, 1060 Vienna, Austria
[b] AC2T research GmbH, Viktor-Kaplan-Straße 2/C, 2700 Wiener Neustadt, Austria

## HIGHLIGHTS

- We use large-scale molecular dynamics simulations to model a grinding process of a ferritic work piece.
- We visualize the microstructural development of a nanocrystalline work piece using time-resolved computational tomography.
- We introduce "differential EBSD tomography" as a tool to detect subtle changes in the grain structure and orientation.
- We elucidate the deformation mechanisms occurring during grinding as a function of load.

## GRAPHICAL ABSTRACT
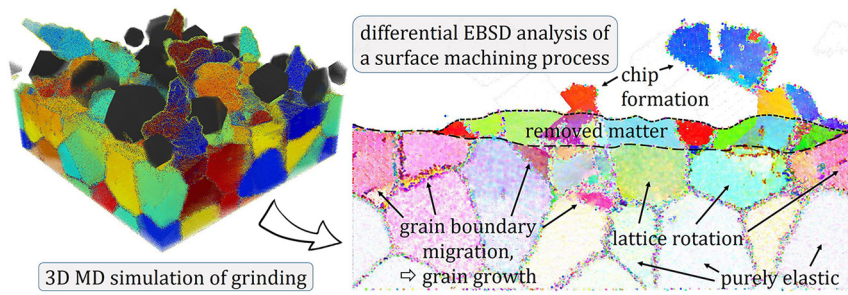
## ABSTRACT

Microstructural changes in the near-surface regions of a material determine its mechanical properties and consequently also its tribological behavior. This work is a study of the microstructural development of nanocrystalline ferrite subjected to a grinding process using molecular dynamics simulations. We visualize the work piece by producing various types of computational tomographic sections that are colored according to the grain orientation, the local temperature, the stress in grinding direction, as well as the atomic flow velocities. In particular, we introduce "differential EBSD" tomographs to highlight the changes to the microstructure caused by the grinding process, allowing us to detect even subtle differences in lattice orientation and small distances in grain boundary migration. We use our visualization approach to discuss the acting microstructural mechanisms in a load- and time-resolved fashion, spanning a wide range of grinding conditions from mild to severe. In addition to removed matter, we observe lattice rotation originating at the surface and advancing deeper into the work piece with increasing load, grain growth by grain boundary migration, and the transient formation of unstable small new grains.

## 1. Introduction

Grinding is one of the machining processes that are known to change a material's structure in the near-surface zone significantly [1–3]. As a consequence, mechanical properties in these near-surface zones such as toughness or hardness are altered, which can change the material's reaction to external loads and thus directly affect its tribological properties [4–6]. Modifications of the microstructure in surface-near zones, such as finely structured surface layers, if caused by sliding with a usually rough counterbody, are also known as tribologically transformed zone (TTZ) [7]. Such layers cannot be described using macroscopic bulk material properties, although their local properties will greatly influence material removal processes or the friction between two surfaces [8]. Tailoring materials and their interacting surfaces to meet specific

requirements during their service life is becoming increasingly important to improve the performance or extend the lifetime of machine parts. Additionally, the machining industry is facing stringent demands regarding the degree of surface smoothness of finished components [9–11] and is exploring novel processing techniques such as rpm-synchronous grinding [12] or fuzzy logic [13] for efficient machining. The technological state of the art has reached a point where further process improvements are only possible with a fundamental understanding of the prevailing mechanisms. Numerous experimental analyses of near-surface zones exposed to machining processes [14] and sliding contacts [15] have shown that the occurring microstructural modifications are restricted to sub-micrometer surface depths. As experimental studies at this length scale are costly and time-consuming, computer simulations have become an important tool to shed light on complex phenomena and to identify the associated mechanisms.

Since the 1990s, molecular dynamics (MD) simulations, which are based on atomic interaction potentials, have proven to be able to reproduce cutting processes and two-body abrasion [16–18], revealing fundamental principles of material removal on the scale of single asperities. In later studies it was demonstrated that plastic deformation processes like dislocation generation can be modeled using (polycrystalline) MD models [19–22]. One important advantage of such an atomistic approach is that it does not require parameters such as activation energies for structural changes like grain growth, or the assumption of constitutive material laws as in continuum mechanics [23–25]. With increasing availability of high-performance computing it is nowadays possible to simulate systems with tens to hundreds millions of atoms within reasonable times (i.e., days to weeks), producing results of surface engineering relevance [26].

Current literature on MD simulations provides tremendous insight into the material behavior on the nanoscale and the microstructural evolution during plastic deformation [27–29]. In tribological contacts as well as during machining processes, the substrate is usually only in contact at the asperity level, assuming that we focus on dry or boundary-lubricated situations [30]. The substrate is therefore repeatedly exposed to non-homogeneous pressure distributions, with time-variable stress conditions applying below the contact regions as the abrasives or asperities of the counterbody pass. This type of stress situation requires a simulation approach that can intrinsically handle non-homogeneous loads to describe the deformation behavior of near-surface zones in the first couple of nanometers. As tribological properties are strongly influenced by the material properties near the sliding interface, this is of great relevance for the friction and wear performance of the material [31]. Here, it is not completely understood if friction and wear are mainly influenced by the grain size or a specific microstructure [28]. Additionally, it has been shown that microstructural changes in a material subjected to grinding or sliding happen at the very beginning of these interfacial processes (i.e., running-in), even after one single pass of the counterbody, making the time span observable with MD reasonable to study such phenomena [32–34].

In previous work [35], we give a comprehensive overview of how MD can be used to model substrates with Gaussian surface roughness and expose them to multi-grit abrasion. Detailed topographic and wear analyses together with a study of the evolving contact areas have shown that macroscopic wear and friction laws are still valid on this reduced length scale, provided that the contact is of a multi-asperity nature [30]. This justifies a reduction of a large grinding system to a nanometer length scale, making it computationally manageable via MD.

Here we study a nanocrystalline work piece that is exposed to recurring indentation, shearing, and scratching by hard abrasives. As a consequence, the grains near the surface are repeatedly loaded and unloaded during the grinding process. The abrasives exhibit a range of sizes and orientations in order to better resemble realistic abrasive morphologies and size distributions. The main focus of our simulations lies in the elucidation of deformation processes occurring in a nanocrystalline work

piece during grinding. Various modes of plastic deformation and structural changes occurring in grinding processes, which depend on microstructural parameters such as grain size or on the local loading history, have already been identified in experimental studies [36,37]. However, it is highly nontrivial to visualize "what happens when" while producing a given surface texture or near-surface microstructure in the absence of costly in-situ methods. This is exactly the research gap that we aim to address with this contribution: to provide a set of visualization tools that give materials scientists the opportunity to look at microstructural data from simulations in a fashion that they are accustomed to, such as EBSD, which is not yet very common in computational materials science. Going beyond that, we provide additional ways of representing microstructures that are tedious or even impossible to obtain from experiments, such as atomic vorticity plots or a superimposed "before/after" imaging technique dubbed "differential EBSD tomography", that can greatly contribute to the elucidation of a mechanism. This has the potential of allowing a highly time-resolved in-depth appraisal of the elementary mechanisms leading to microstructure evolution at the early stages of surface machining. In this work, we apply this set of tools to explore which of the above-mentioned plastic deformation modes can be reproduced using large-scale MD simulations at the example of nanoscopic grinding of a ferritic iron work piece.

## 2. Simulation and visualization details

All our simulations were carried out using the open-source MD code LAMMPS [38]. The exact procedure of our model construction is described in earlier work [39]. It consists of a $60 \times 60 \times 20$ nm³ $\alpha$-Fe polycrystal with a rough surface and 18 randomly oriented and distributed rigid truncated-octahedral abrasives with Gaussian size distribution, see Fig. 1a. The grains in the work piece have a mean grain diameter of 12.7 nm and are initially randomly oriented, and the surface topography has a fractal dimension of 2.111, an RMS roughness of 0.7 nm, and a lower frequency cut-off producing a typical lateral roughness feature extent of 23 nm. The atoms located in the lower 3 Å of the simulation box are kept rigid to emulate bulk support. The system was heat treated by ramping the temperature from 0 K to 800 K over 180 ps, then keeping it at $T = 800$ K for 800 ps, followed by linear cooling to 300 K over 200 ps, holding $T = 300$ K for another 400 ps. The heat treatment is controlled by a Langevin thermostat with a time constant of 0.5 ps, acting on the entire system during the temperature ramps, but only on three monolayers of Fe at the system base in the constant temperature phases to allow unconstrained local relaxation. The Fe—Fe interactions are governed by a Finnis-Sinclair potential [40].

The 18 abrasives are based on a bcc lattice with the (100) and (111) planes acting as crystallographic cleavage planes to give the abrasives their final appearance. They have diameters ranging from 6 to 14 nm, with the mode of the distribution at 10 nm, leading to an effective projected surface coverage of 37%. The chosen abrasive size distribution constitutes a trade-off between computational manageability, the desire to include several abrasives so that the relative orientation of a single one does not have excessive impact on the overall results, as well as attempting to keep the ratio between abrasive and grain size close to 1. As in [41], the interactions between abrasive particles and the Fe surface are modeled using a Lennard-Jones potential with the parameters $\varepsilon_{LJ} = 0.125$ eV and $\sigma_{LJ} = 0.2203$ nm. These values are similar to [42,43] and yield an interaction roughly one order of magnitude weaker than the one for Fe—Fe, which means that there will be some adhesion between the abrasives and substrate as well as the wear particles. The abrasives are pulled across the surface at a sliding velocity in $x$ direction of $v^{(abrasive)} = 80$ m/s and an angle of 6.42° with the $x$-axis, so that they re-enter the simulation box at different $y$ positions every time they pass the periodic box boundaries and therefore never follow exactly in their own grinding paths. The relative abrasive positions are locked throughout the simulations, and abrasive rotation is disabled, resembling a two-body process with bound grains. Furthermore, the abrasives
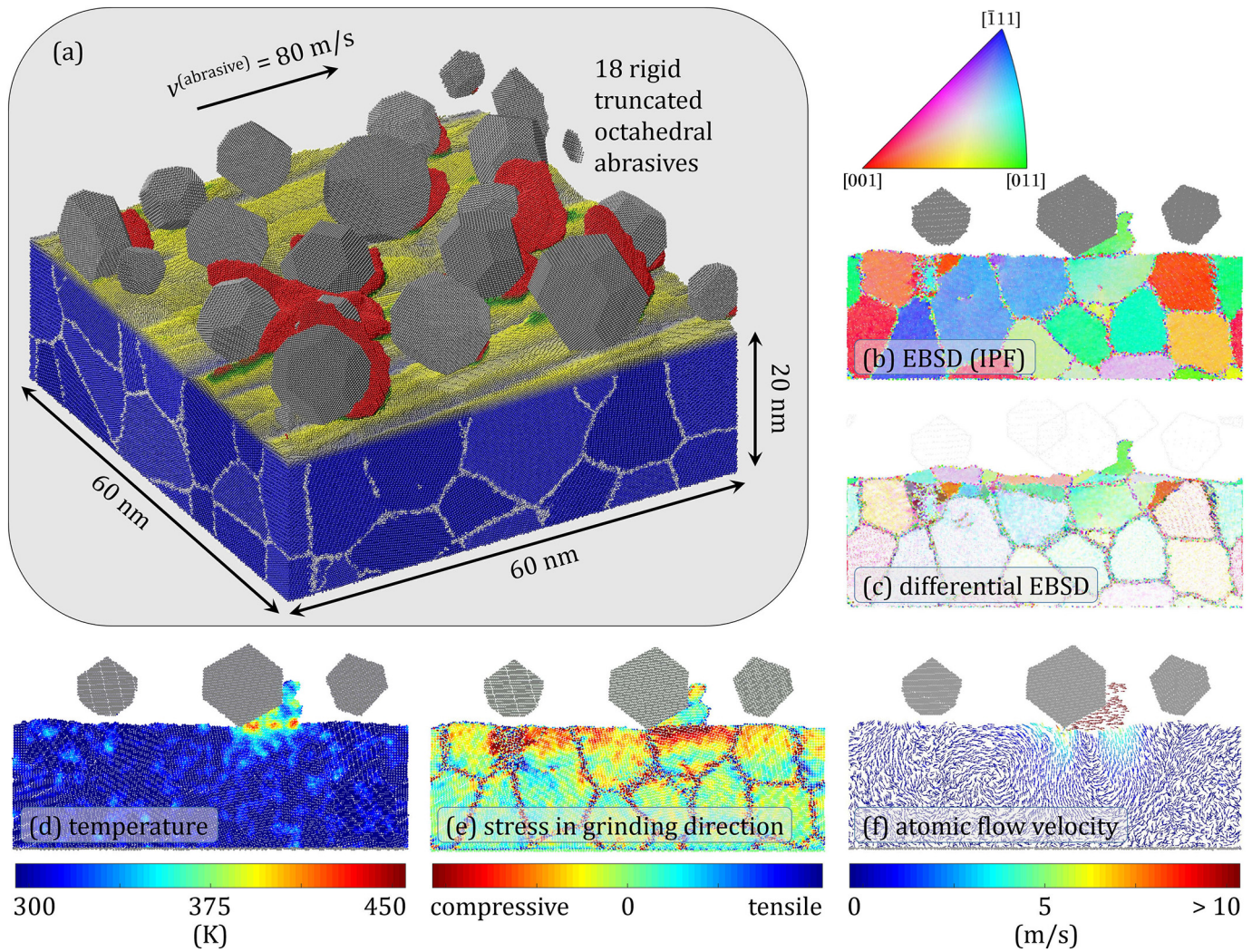
**Fig. 1.** (a) 3D representation of the MD system after 5 ns of grinding. Grains are blue, grain boundaries white, abrasives gray, the surface yellow/green, and the abraded chips red. Five representative computational tomographic 2D-sections are shown in panels (b–f) to give an overview of the visualization modes discussed in detail later on in this work.

can change their $z$ position collectively depending on the topography, similar to a grindstone, but not individually as in a slurry. Because of their rigidity, the abrasive particles themselves are not subject to any wear, which is a simplification over real systems, but reflects the fact that abrasives are typically much harder than the work piece. The normal pressure $\sigma_z$ on the abrasives (defined as the total force in $-z$ direction acting on the abrasive particles divided by the lateral cross-section of the simulation box, 3595.4 nm$^2$) is kept constant at values ranging from 0.1 to 0.9 GPa for a simulation time of 5 ns. While it is non-trivial to experimentally measure contact pressures during grinding due to the uncertainty in the contact area, our assumed values correspond to the range encountered during the running-in period of a grinding process [44,45], where, depending on the infeed depth, an initial pressure spike of up to 1.5 GPa will typically relax to below 0.1 GPa.

The electronic contribution to the thermal conductivity $\kappa(T)$, which dominates in metallic systems, is not accounted for in the interaction potentials applied in classical MD. In this work, we adopt the concept of electron-phonon coupling as laid out in [46,47]. This does not require us to implement a time-consuming multiscale approach, but rather assumes that due to their high mobility within the metal, the electrons can be used as an implicit heat sink permeating the substrate. In a separate publication dealing with these aspects [48], we described how we calculated $\kappa(T)$ for several values of the Langevin thermostat coupling

time $\lambda$ and found that the best reproduction of the experimental thermal conductivity of Fe [49] can be achieved with $\lambda = 3.5$ ps throughout our desired range of normal pressures. During the grinding simulations, the Langevin thermostat acts only in $y$ direction, (nearly) perpendicular to the directions of normal pressure and grinding, so as not to overly interfere with the imposed constraints of normal pressure and sliding velocity. An additional benefit of this thermostatting scheme is that the cooling of the removed matter (e.g., via a coolant fluid) is, at least for all practical reasons, accounted for in this way, i.e., even if the chips are already detached from the work piece surface and have no more thermal coupling to the base thermostat, they can cool off by themselves.

The majority of the computational tomographs of the work piece shown and discussed throughout this work are colored according to grain orientations as in electron backscatter diffraction (EBSD), using the inverse pole figure (IPF) coloring standard, see Fig. 1b. The orientations were calculated using polyhedral template matching [50] as implemented in OVITO [51], and the color rendition was carried out using the MTEX toolbox [52,53] for Matlab. As some of the microstructural changes in the system, especially migrating grain boundaries and slight lattice rotations, can be rather subtle, it has proven valuable to also produce differential EBSD images, comparing the structure of a given time step with the initial one, as shown in Fig. 1c. This can be

carried out in an image processor such as GIMP, where the image in question is exactly superimposed over the initial configuration as a layer. For producing clearer results, the abrasives are first selected using a color selection tool (we used a threshold value of 5), which allows the deletion of entire abrasives without introducing artifacts into the representation of the work piece. Then a difference filter is applied to the top layer, which calculates the absolute value of the difference between the RGB values of all superimposed pixels (and is therefore commutative), the result of which is then inverted to return to the original EBSD color scheme. The resulting representation of the system is nearly white in all regions where no changes occurred and colorful in regions that changed by a large amount, with pastel hues where changes were slight. It is therefore perfectly suited for identifying small changes in the surface topography, deviations in the courses of grain boundaries, and especially lattice rotations. Note that once changes have been identified using this visualization, the respective EBSD image has to be revisited for a proper discussion of the results, as the differential image may obscure which feature belongs to which configuration.

When visualizing the temperature in a system where portions move at velocities comparable to thermal movement (of the order of 100 m/s), it is important to first filter out any advective component of atomic translation. One straightforward way of doing this is defining a control volume around every evaluated atom and calculating the mean velocity of this control volume. The choice for the size of the control volume is a trade-off between accuracy and spatial resolution, and we found that a radius of 1 nm around each atom includes a sufficient number of atoms within each control volume for filtering out the advection velocity effectively. Although this leads to a slightly patchy temperature map with a minimum feature size of the projection of the control volumes onto the plane of the tomographic slice, it is clearly discernible where the hot spots are located and how the heat is dissipated from the contact interface, see Fig. 1d.

LAMMPS can calculate per-atom stresses, making it possible to produce visualizations of the distribution of any stress tensor component, as shown in Fig. 1e for the principal stress in grinding direction. There are, however, some caveats: first, the quantity calculated by LAMMPS is actually a per-atom stress multiplied by the volume that the respective atom occupies, with the latter of the two possibly not being well-defined in a strongly sheared solid. Second, the output at the temperatures occurring in our systems is strongly degraded by thermal noise, so any snapshot of the system that should be evaluated in a time- and space-resolved fashion needs to be re-read, energy minimized, and re-written before it can be post-processed. These restrictions aside, obtaining a general idea of the stress distribution within the grains that trigger processes leading to microstructural changes is highly instructive, even if the values cannot be exactly quantified.

The last mode of visualization applied in this work is a representation of the atomic flow velocities, see Fig. 1f. By calculating the mean velocity of a subset of atoms (e.g., every fifth atom) from two snapshots that are 40 ps apart, all thermal noise is automatically filtered out, and the velocity vector can then be plotted at the position of the respective atom at the time step exactly in-between. Normalizing the vector length and rather coloring the vectors according to their norm produces a vector map of the atomic flow velocities. This representation can be considered the complementary view of the thermal visualization shown in panel d. The output is then optimized for analyzing the "slow" processes occurring within the work piece (as opposed to the fast movement of the chips being abraded from the surface) by limiting the color map to 10 m/s. In this way it is possible to make visible the formation of vortices preceding the rotation of the lattice in a grain, or steep intragranular velocity gradients that are followed by the formation of a grain boundary.

## 3. Results and discussion

A typical series of cross-sections through the substrate after nano-abrasive grinding is shown in Fig. 2, where we qualitatively compare microstructures after grinding at normal pressures $\sigma_z$ ranging from 0.3 to 0.9 GPa. Our simulations show that the changes of the microstructure due to grinding strongly depend on the applied normal pressure. Under the mildest simulated conditions below 0.3 GPa, there are hardly any observable changes in the microstructure, although the initial topography is somewhat smoothed. With increasing normal pressure the chip volume grows considerably, and pronounced grinding grooves are formed on the work piece surface. The bird's eye view in Fig. 1a shows the numerous parallel grooves generated during grinding. Despite this groove formation, the surface is smoothed by grinding, with the RMS roughness decreasing to 0.4–0.6 nm at the end of the simulation from its initial value of 0.7 nm for all but the highest normal pressure. Comparing representative slices to the corresponding slice in the initial structure makes it easier to identify changes. Therefore, the following figures only show selected positions at different normal pressures to best illustrate various features. Furthermore, the differences between the initial configuration and the respective final configuration at the various normal pressures are shown in the differential EBSD visualizations to emphasize the changes during the grinding process. Here regions without change are colored in white, whereas more stronger hues represent greater changes between initial and final configuration.

At the lowest normal pressure of 0.3 GPa, a change in surface topography (i.e., smoothing) by wear of asperities is shown in Fig. 2. Especially interesting positions are annotated with numbers. Very small grains such as the purple (235) one (grain number 1 in Fig. 2) contained in these asperities disappear completely upon contact with the abrasive particles, independent of their initial orientation. If the infeed depth of the abrasives is sufficiently high, these grains are taken away during a single pass of an abrasive. Other grains such as the small blueish (245) grain (number 2 in Fig. 2) in the middle of the slice also seem to disappear, but still exist in a neighboring slice that is not shown here, indicating lateral grain boundary migration.

It is worth mentioning that the infeed depth does not exceed the size of the small grains within the asperities. They are not entirely worn off, but the remains of the small and partly abraded grains are incorporated into the neighboring grains by grain boundary migration, analogous to what is reported in [27]. Thus, as the smaller grains vanish, the larger neighboring grains and the ones below the asperity grow to the surface, but retain their initial orientation.

Similar observations regarding the abrasion of asperities can be made for an increased normal pressure of 0.6 GPa. However, as a result of the greater infeed depth for higher loaded processes and as a consequence of the greater energy introduced into the system, the removed matter depth is increased and larger portions of the the near-surface grains are worn off. Therefore, more small grains vanish and more surface asperities are removed, as can be seen when comparing the EBSD and the differential EBSD tomographs in the center and right column of Fig. 2. The comparison of the microstructural evolution of the same tomographic section subjected to different normal pressures in Fig. 2 shows that the grain size has to fall below a certain critical size in order for the smaller grains to vanish (e.g., the green (157) grain (number 3) in the middle of Fig. 2). In addition to grain growth, lattice rotation induced by the sub-surface shear stresses can be observed at the higher load of 0.6 GPa and even more so at 0.9 GPa. This lattice rotation can also result in grain growth, as the grain boundary is eliminated when two grains coalesce through rotation (not shown here), leading to a decrease in the total grain boundary energy and stress concentration [54]. In terms of grain growth the dependence on normal load is consistent with earlier theoretical and experimental studies by Pan and Rupert [55] as well as Argibay et al. who also showed more grain growth for higher loads [56]. The effect of increasing normal pressure can also clearly be seen in the visualization of the differences between the initial and the respective final configuration at varying normal pressures in the right column of Fig. 2. At 0.3 GPa, only a thin layer of the surface is worn off, and virtually no microstructural changes can be observed. With increasing normal pressure the removed matter depth
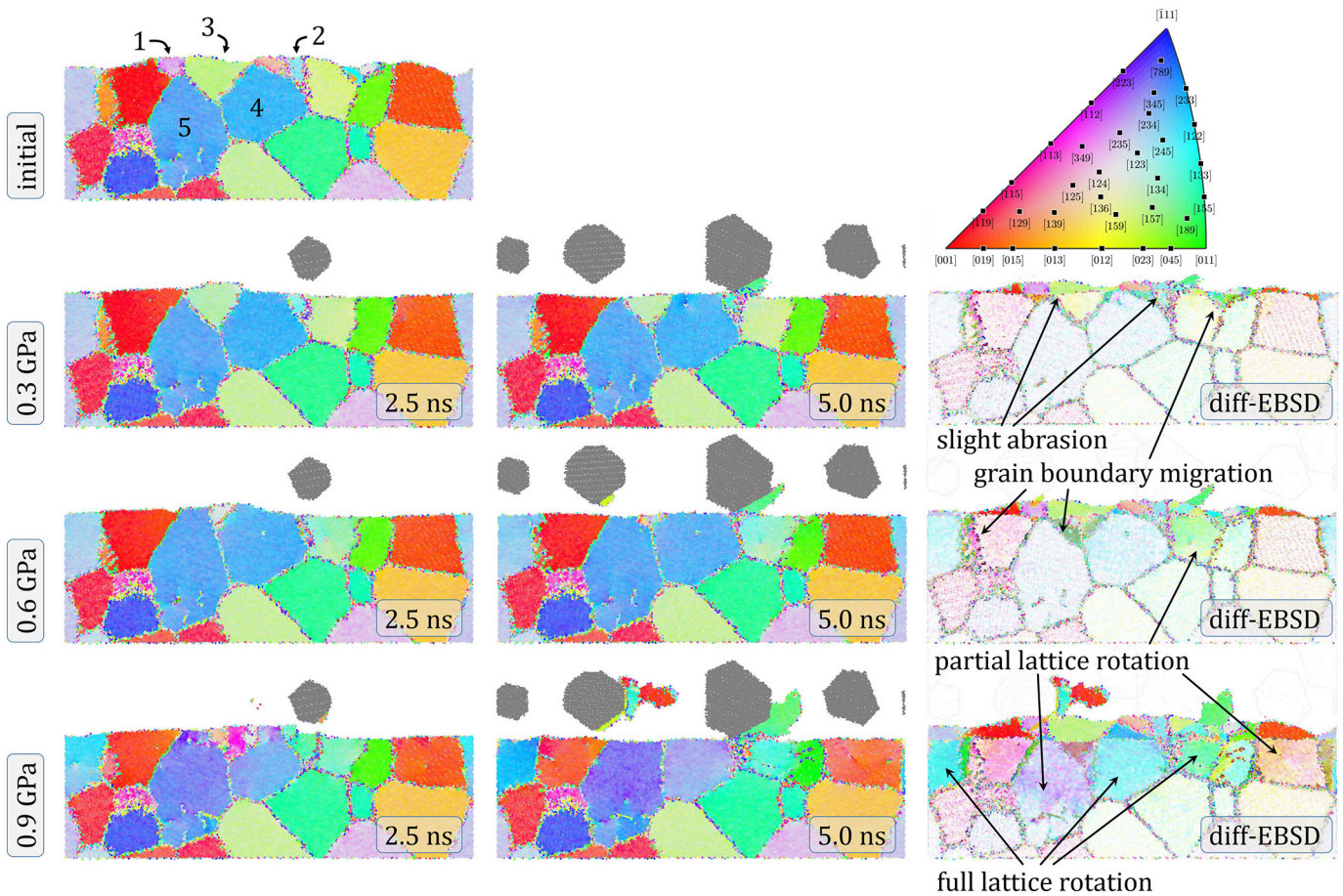
**Fig. 2.** Normal pressure dependence of the microstructural development of a representative computational tomograph. The left two columns show EBSD visualizations of the initial configuration and after grinding for 2.5 ns and 5 ns at 0.3, 0.6, and 0.9 GPa. The right column is a visualization of the differences between the respective final and the initial configurations ("differential EBSD"), indicating material removal, chip formation, lattice rotation, and grain boundary migration. Note: the colors in these *differential* EBSD images do not correspond to orientations in the legend.

is increased, which is reflected in the strong colors of the topmost layers. Additionally, incipient lattice rotation can be observed in the form of slight color changes at 0.6 GPa. Finally, strong colors for the highest normal pressure of 0.9 GPa indicate pronounced lattice rotation. This rotation can affect an entire grain as in the right blue grain (grain number 4), where the homogeneous blue of the initial (233) orientation changes to purple (223). On some occasions, even the largest grains in the substrate may sequentially change their orientation completely by rotation when the grain is passed repeatedly by abrasive particles. For other large grains, as the left blue grain (grain number 5), the hue varies slightly even within the grain as the bottom part remains almost in its initial orientation, whereas the upper, sheared part rotates towards purple. The differential EBSD images in the right column of Fig. 2 clearly show that all microstructural changes happen only in the topmost layer of the work piece, which is in direct contact with the abrasive particles since the bottom grains are all white and hence did not undergo any lattice rotation. This is in good agreement with the results from Pan and Rupert, who also demonstrated in their MD study of nanocrystalline Cu subjected to sliding that the microstructural changes (i.e., grain growth) are confined to the near-surface regions [55].

Similar to the present study, microstructural evolution in the course of plastic deformation of nanocrystalline metals has already been observed in various experimental and theoretical studies, leading to the conclusion that grain growth results from a combination of grain boundary migration and grain rotation. Jin et al., for example, proved this mechanism of grain growth via a TEM analysis of ultrafine-grained Al during nanoindentation [57]. Grain growth upon sliding of nanocrystalline materials was also observed by Rupert and Schuh, who investigated the microstructural evolution of Ni—W during sliding. They could show that grains larger than 10 nm do not undergo microstructural changes upon sliding, whereas grains smaller than 10 nm show grain growth, which is mechanically driven by high near surfaces stresses, causing grain boundary migration and grain rotation [58]. Furthermore, Romero et al. demonstrated local grain growth and merging of grains in an iron tribosystem during sliding using MD simulations [27]. They concluded that asperity interlocking leads to grain rotation and plastic deformation, followed by grain boundary migration from smaller grains to larger grain boundaries, initiating grain growth. In their study, in accordance with the present study, the smaller grains vanished in favor of the larger grains.

A reduction in grain size by wearing off parts of the grains during grinding is inherently accompanied by a higher fraction of high-energy grain boundaries. As a result, the small abraded grains become energetically unstable, and the grain boundaries of these grains move towards the surface or towards the sides, parallel to the sliding direction, triggering grain growth, similar to what is discussed in [59]. With increasing normal pressure, the grain boundaries can traverse larger distances. Thus, the main driving force for grain growth is the reduction of grain boundaries to reduce internal energy. None of our simulations, which all started from the same random texture, indicated that a specific grain orientation would grow preferentially.

Beyond grain growth we also observed the generation of new grains at the surface that are smaller than the average initial grains. Examples of such grain refinement can be found in Fig. 2 at 2.5 ns for the highest

pressure of 0.9 GPa. Though not shown here, the generation of smaller grains can also occur at smaller normal pressures. The grains form when an abrasive passes and exerts a shear stress on the substrate that is sufficient to make the grain or parts of grains beneath the abrasive rotate by such a large angle that a new grain boundary is formed.

Monitoring the microstructure throughout the grinding process, these newly formed grains appear at random times throughout the grinding process. However, analogous to the initially existing small surface grains, they proved to be unstable in all our simulations, and they vanish either as soon as the abrasive has passed, or at the latest when the following abrasive passes the respective position. A new rotation process is then triggered, which makes the newly formed grain boundary disappear again, and the adjacent larger grain reincorporates the surface grain. This course of events prevents the formation of a persistent or continuous nanocrystalline layer, which has also been observed after sliding experiments [8,31]. However, as the average grain size is already quite small at 12.7 nm, and similar grain sizes have been found after sliding of nanocrystalline metals, this is not entirely surprising [55].

As already mentioned, apart from grain size changes, the local orientation of the growing grains can change as well. This can be clearly observed in the differential EBSD images in Fig. 3. At the smallest investigated normal pressure of 0.1 GPa, the shear stresses exerted on the surface grains are not sufficient to induce grain rotation. However, upon increasing the pressure to 0.3 GPa, grain rotation of the smallest grains sets in. In this context, it has been shown that for GB diffusion dominated processes, there is a $d^{-4}$ dependence of the rotation rate on the grain diameter $d$ [60]. Therefore, grain rotation is much faster for the smallest grain sizes, where deformation is mainly accommodated by grain GB diffusion. Additionally, our investigations show that there is a dependence of the propensity of lattice rotation on the initial grain orientation. We observe that blue or purple grains corresponding to initial orientations between (112) and (111) seem to start rotating at lower normal pressures than other grain orientations. As in Fig. 2, we could also observe grain growth by grain boundary migration for normal pressures from 0.3 GPa as well as chip formation during the abrasion process. Both effects are enhanced with increasing normal pressure, resulting in larger grains and the formation of larger chips, which is in accordance to earlier studies [55,56]. When the normal pressure is increased to 0.6 GPa, the shear stresses are high enough to induce lattice rotation also in the larger grains and those with orientations deviating from blue or purple. This trend continues until, at the highest pressure of 0.9 GPa, most surface grains undergo lattice rotation. The observation in our simulations that larger grains rotate at higher pressures agrees well with previously made experimental observations in nanocrystalline metals showing a $d^{-4}$ dependence of the rotation rate on the grain size [60,61]. Additionally, Vo et al. made similar observations in their MD study and showed increasing grain rotation with higher strain in nanocrystalline Cu during plastic deformation [62].

A slight color gradient within one grain without any formation of a grain boundary or dislocations, as can be observed for 0.9 GPa in Fig. 2 (grain number 5) and Fig. 3 (pink grain number 6), indicates local lattice tilts, leading to intragranular elastic strains. In the demonstrated cases, where blue changes from (233) to purple (223) and pink from dark (349) to light pink (124), a generation of preferred (111) orientations of surface grains due to grinding, or a common rotation towards (111) cannot be confirmed. We cannot exclude that the simulations might be too short or the loading conditions too mild to reproduce such a texturing effect that is sometimes reported in experimental studies [63]. Note that the local directions of the principal stresses are not constant, since the rake angles differ between abrasives, and they vary over time as the asperity angles change during grinding. Thus, the orientations of most preferred slip planes according to Taylor's law will change constantly.

At higher normal pressures, the friction energy introduced into the system increases, so the temperature in the sliding interfaces is expected to rise as well. As it is known that frictional heating and highly localized deformation are the main driving forces for microstructural evolution [58], and since temperature is one of the key quantities that can determine grain boundary mobility, we also investigated the effect of temperature, see Fig. 4. Throughout all simulations, large portions of the work piece remain below 320 K due to the adopted thermostatting procedure that emulates a well-cooled process [48]. Consequently, the generated heat is quickly conducted away from the sliding interface, where the bulk work piece as well as the chips act as heat sinks. Only in the high-load cases above 0.6 GPa, the sliding interface between the chips and the work piece heats up to beyond 450 K. At the highest normal pressures, short-lived temperature spikes reaching up to 750 K can occur at edges of abrasives, but these do not extend beyond 2 nm from the contact point. Overall, the volume heated above 400 K remains small, and the affected region is limited to zones close to the surface. Additionally, the work piece quickly cools down to at least 350 K between two passing abrasives, even at 0.9 GPa, so there is never any appreciable accumulation of heat at the surface, cf. the top right panel in Fig. 4. When comparing the extent of the regions that underwent microstructural changes, i.e., the grains with strong hues in the differential EBSD image, with the extent of the heated regions in the right column, it becomes clear that the mechanical energy introduced into the system dominates any thermal influence. This agrees well with a time-dependent analysis of the local stress distribution of the respective tomograph, which proves that the highly stressed regions extend all the way down to the lower grain boundary of near-surface grains while an abrasive is passing, especially when it is pushing removed matter in front of it. This can be seen in the central bottom panel of Fig. 4, which shows an earlier event where a stress peak permeates an entire grain that is then going to be plastically deformed. The corresponding thermal analysis of the same time step in the bottom right panel clearly shows that the more strongly heated regions are confined to within approximately 1 nm of the sliding interface, and the depth to which microstructural changes occur exceeds the strongly heated regions by a factor 2–3 in this example, or even by a factor of 10 or more in larger grains. We can therefore neglect any increased grain boundary mobility due to higher temperatures or any annealing effects within the work piece, so the observed microstructural changes can be traced back to mechanical deformation.

Finally, all microstructural changes observed during the grinding process at the highest pressure of 0.9 GPa are summarized in Fig. 5, which gives a chronology of events. In the initial configuration before grinding, shallow surface grains, such as the pink (125) one (grain number 7), are still visible. These small grains are abraded in the first steps of the process, sometimes even by a single abrasive particle, depending on the infeed depth, which is in line with the phenomena reported after a single pass of a single asperity in [31,32]. Additionally, first signs of lattice rotation can be observed, for example, in the yellowish (159) grain (grain number 8) bordering the shallow pink grain, which rotates towards green (134). This rotation happens during the first pass of an abrasive, during which also the light pink (125) grain (grain number 9) is worn off, with its remains being incorporated into the neighboring yellow grain by grain boundary migration, resulting in grain growth. After a few passes of abrasives, the small surface grains are completely removed, and the larger grains below have grown to the surface.

Apart from grain boundary migration and lattice rotation, plastic deformation is also mediated by dislocations that relieve plastic strain introduced by external loads. The latter vary considerably in time and space as the contact with randomly oriented abrasives is highly nonconformal. Dislocation motion can be seen in the EBSD tomographs, especially when viewed as a movie (see the Supplementary Material), and a more detailed dislocation analysis (DXA) carried out in OVITO [64] revealed that they originate at the surface just underneath the passing abrasives. The majority of the grains are not large enough to contain intragranular Frank-Read dislocation sources and therefore
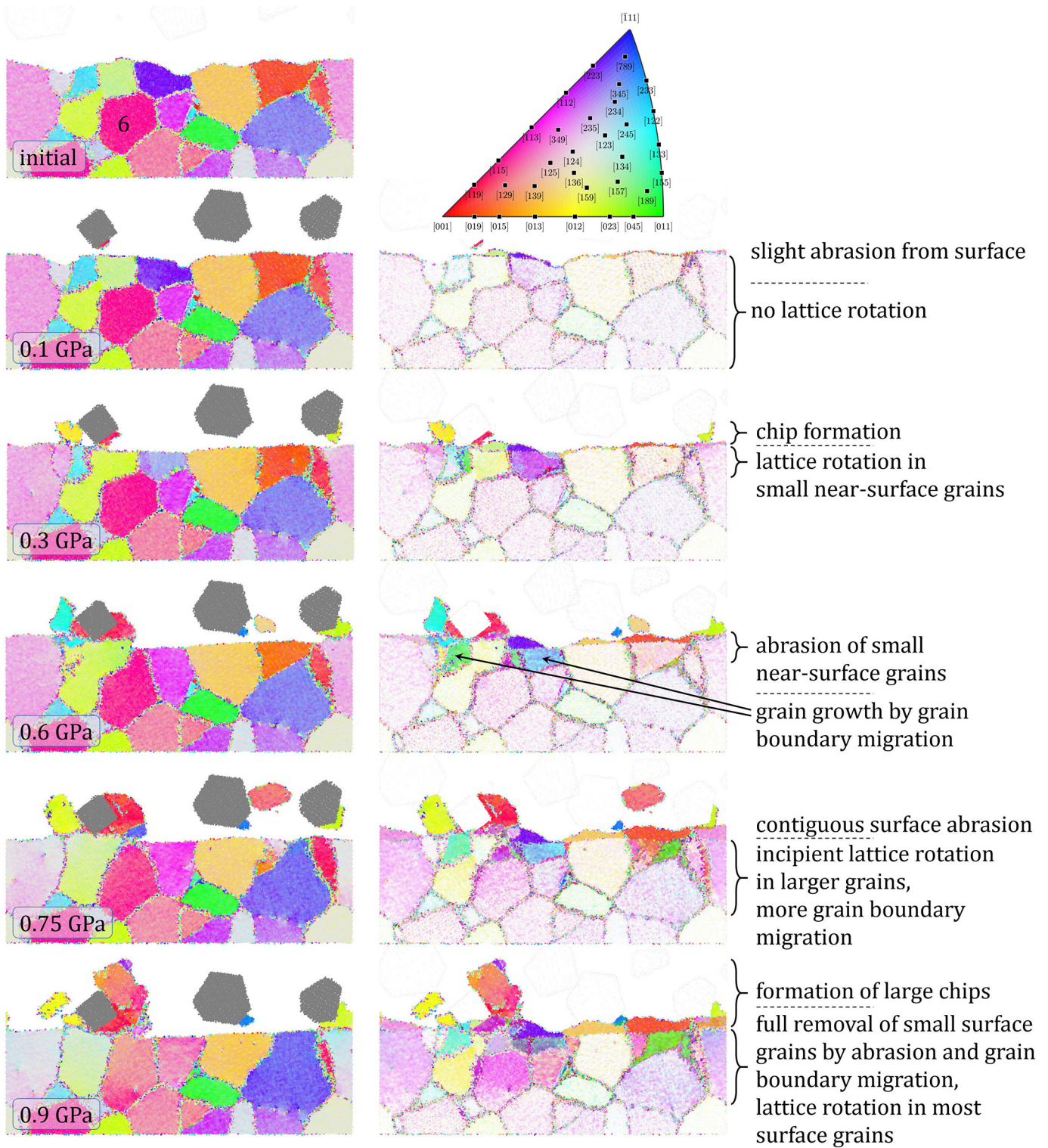
**Fig. 3.** Load dependence of microstructural changes during grinding. Left column: EBSD images of initial configuration and after 5 ns of grinding at several normal pressures. Center column: differential EBSD images highlighting the microstructural changes.

cannot emit dislocations. In this context, Ohashi et al. showed that the shear stress necessary to emit a dislocation from a Frank-Read source increases sharply when the grain size approaches the size of the Frank-Read source [65]. The dislocations emitted from the surface into the larger grains are quickly annihilated or move back to the free surface as soon as the abrasive has moved on, since the grains are not large enough to store them [66]. Only the largest of the grains

in our system have the ability to store several dislocations for longer periods, an example of which can be seen in the large blue (345) grain (grain number 10 in Fig. 5). However, the generation of dislocations can also lead to grain fragmentation, as can be seen in the smaller blue grain in the middle (grain number 11). After the small surface grains have been removed, the next abrasive, pushing removed matter in front of it, generates a high stress field inside the
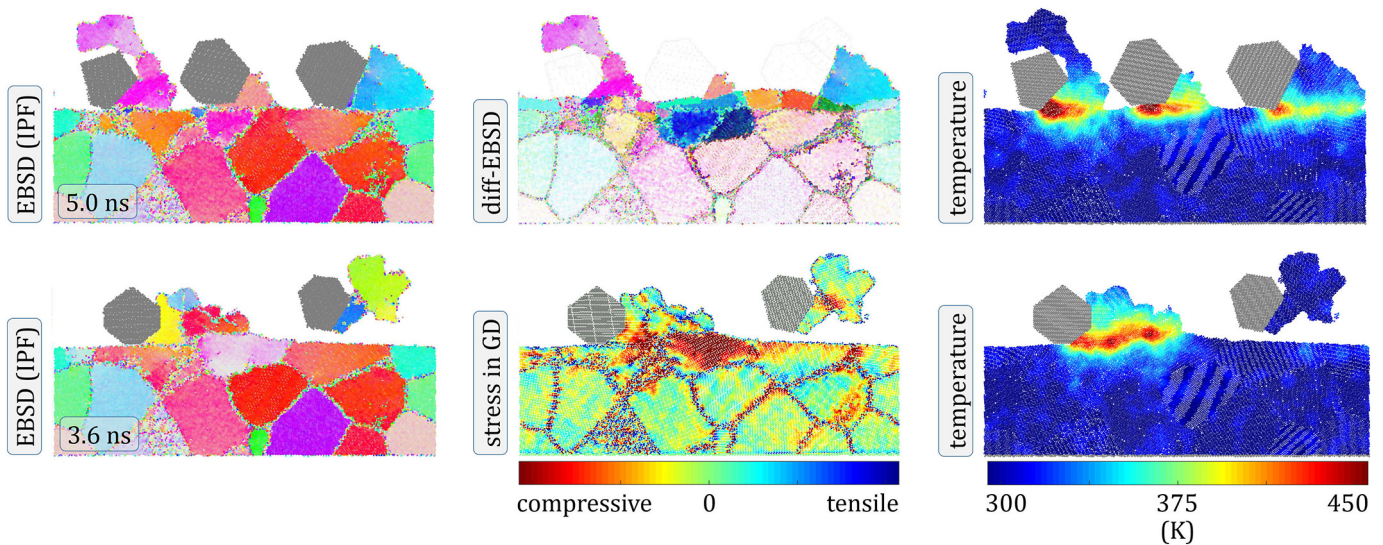
**Fig. 4.** Thermal and stress analysis of a representative tomograph after grinding at 0.9 GPa. The top row shows the final configuration with the corresponding differential EBSD image, while the bottom row compares the size of the mechanically and thermally stressed regions at $t = 3.6$ ns, when the central pink grain undergoes considerable plastic deformation.

grain at $t = 1.4$ ns. Resulting from this stress accumulation, dislocations are emitted at the surface, which then move through the grain, decreasing and increasing in number over time, eventually forming a low angle grain boundary (LAGB) and thus fragmenting the grain at $t = 1.5$ ns. Simultaneously, the atoms start flowing in clockwise vortex patterns, leading to lattice rotation of the upper part from blue (345) to purple (112), with the bottom part remaining near its original blue. After this rotation, most of the stress in the grain is released. However, with the next incoming abrasive the process is repeated, resulting in a further lattice rotation of the top part towards an orientation shown in light blue (123), most likely around the (111) axis, thus forming a high angle grain boundary (HAGB). The respective changes in the orientation over time can be observed in the orientation maps next to the EBSD tomographs in Fig. 5. In the end there are hardly any dislocations left in both fragmented grains, as the subsequent rotations seem to have largely reduced the stored internal strain and left a nearly defect-free lattice behind. Although this new light blue grain seems large enough to remain stable, it does not survive until the end, since a large abrasive pushing a chip in front of it passes at $t = 4.82$ ns, causing another fragmentation of the grain (further grain refinement) and a rotation of the remaining part towards green (157).

The above means that we do not observe classical strain-hardening effects resulting in nucleation and grain growth after a critical dislocation density has been obtained in the grains, following the Hall-Petch hardening law [67]. Our large-scale polycrystalline MD simulation aids the identification of the acting deformation mechanisms. With its grain diameters limited to keep the system size computationally manageable, our system seems to be located in the transition region between nanocrystalline deformation behavior and dislocation-mediated processes with shear along crystallographic planes. Larger grains feature some dislocations, but these are almost all volatile, moving quickly through the grain or back to the surface or a grain boundary. Studying their time evolution would require the analysis of geometrical snapshots every ~250 fs, corresponding to 80 times our current output rate, which would have prohibitively increased the data storage requirements and post-processing effort.

Overall, the work piece did not exhibit significantly more dislocations at increasing normal loads. As the temperature varied by less than 50 K throughout the largest part of the substrate thickness, it can

be effectively excluded as a determining factor for defect densities. It seems that the grains are just small enough to reduce external strains by rotation, which agrees well with our initial average grain size of 12.7 nm being close to the Hall-Petch breakdown of iron at 14.7 nm [68].

The microstructural changes observed here correspond well to earlier experimental and theoretical findings. These changes are triggered by near-surface shear stresses and include both grain growth and grain refinement as a result of lattice rotation, grain boundary migration, as well as dislocation-mediated processes. This is of high relevance for the mechanical behavior as well as the friction and wear performance of materials like nanocrystalline metals as it determines the material's response during grinding or in tribological applications [8,69]. Naturally, the microstructural evolution in the first stages of cyclic loading in grinding or tribological applications comprising both grain growth and grain refinement will have a major effect on the subsequent friction and wear behavior. Depending on the operating conditions and material pairings, it has been shown that such microstructural changes can lead to a reduction in friction and wear [8,27,55], but also an increase to a high friction state in the course of mechanical loading [58].

## 4. Conclusion and outlook

In this study, we showed that we can use large-scale MD simulations to reproduce near-surface microstructural changes observed in experimental tribological or grinding studies. This is highly relevant since the near-surface microstructure can strongly influence the material behavior and thus its behavior during grinding or sliding processes. To further improve these processes, material removal mechanisms must be understood on a nanoscopic scale, where our MD simulations could make an important contribution. As it is known that temperature is one of the key quantities influencing microstructural evolution, a precise reproduction of how the generated frictional heat is dissipated had to be guaranteed. With the model presented here, thermal influences could be precisely reproduced, showing that the mechanical energy introduced into the system greatly dominates the thermal influence. Thus, concentrating on the mechanical contribution, we systematically studied and visualized the influence of normal pressure and grinding time using MD simulations. In contrast to experimental work, identical initial microstructures can be loaded with a range of
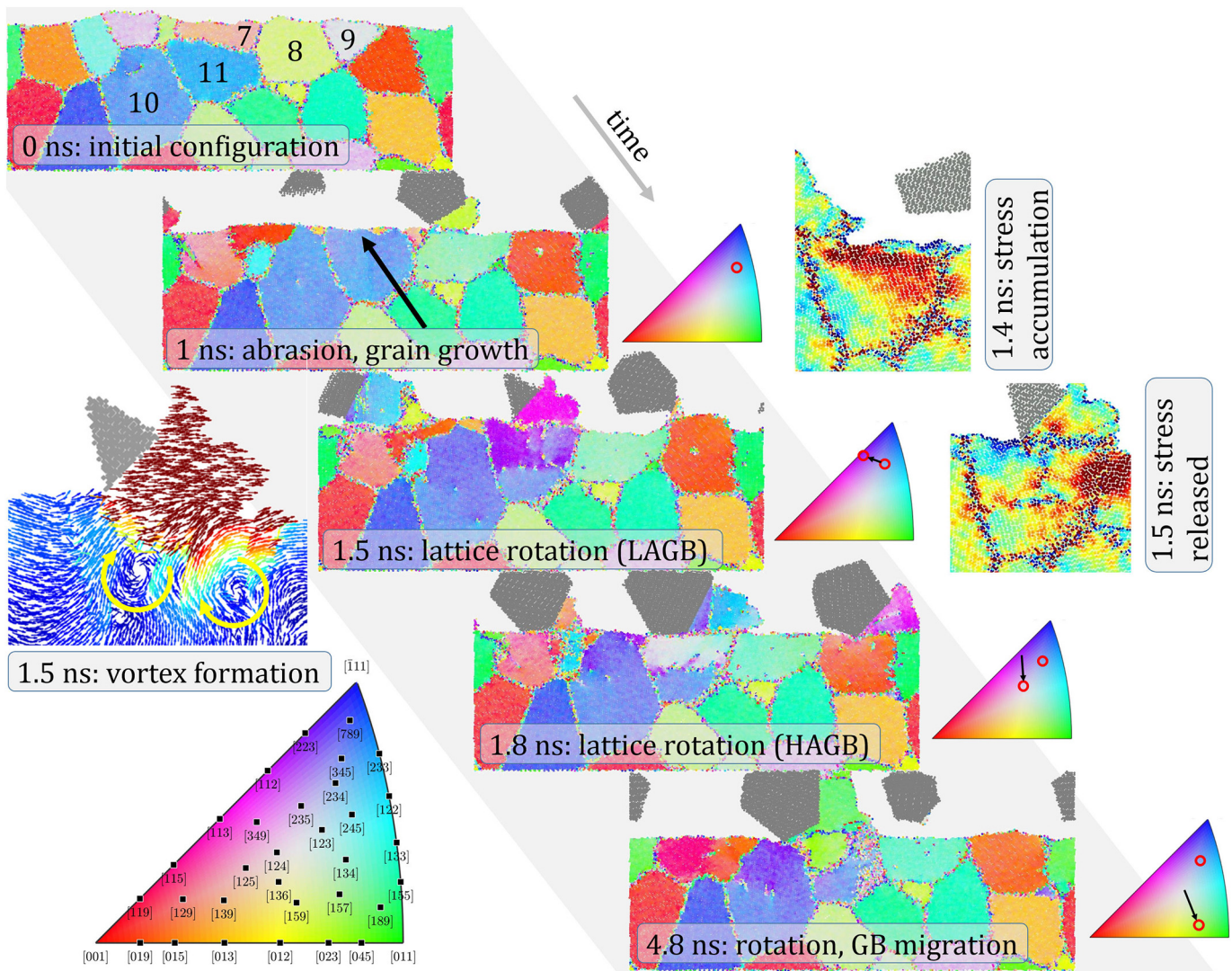
**Fig. 5.** Chronology of abrasion, grain boundary migration, lattice rotation, and grain boundary formation during grinding at 0.9 GPa. The orientation maps next to the EBSD tomographs illustrate the orientation changes in the central blue grain (#11) over time. The stress fields ($\sigma_{xx}$) before and after the first principal morphological change at $t \approx 1.5$ ns are supplemented by an atomic flow map visualizing the vortices that lead to lattice rotation.

different pressures in our simulations. Furthermore, the running-in period (first passes of the abrasives) could be investigated in a highly time-resolved manner. As most of the microstructural changes can be expected during running-in, thus defining the material response to ongoing mechanical loading, our MD simulations could contribute to understanding the governing mechanisms. Here in particular, the microstructural development of a nanocrystalline ferrite subjected to grinding as a macroscale machining process was studied, but the general behavior likely applies to most nanocrystalline metals.

The following conclusions can be drawn:

- The load dependence was studied between 0.1 GPa and 0.9 GPa, which are typical values for the run-in period during grinding and therefore representative for our study. An increase in load leads to a higher chip volume and significant grinding marks. Higher infeed depths at greater loads result in more small grains vanishing that are incorporated into larger neighboring grains. Grain growth is mainly observed in the form of grain boundary migration.
- Above a certain load lattice rotation induced by sub-surface shear stresses can be observed starting from the surface and subsequently progressing into the work piece.

- A transient formation of small and unstable grains (smaller than the initial ones) can be detected. Here, grain parts or entire grains rotate so much that new grain boundaries form. Repeated sliding of abrasives over these newly formed grains leads to the vanishing of the grains, therefore no continuous nanocrystalline layer evolves.
- A thermal analysis of the investigated system clearly showed that the mechanical energy input dominates any thermal influence. There is no heat accumulation, and the temperature only briefly and locally rises to 450 K in the sliding interface between the chips and the work piece. The depth up to which the microstructural changes extend is much larger than the heat-affected volume, which is typically confined to a few nm.
- There is no observation of classical strain-hardening effects such as the Hall-Petch hardening law, as dislocations cannot be stored or even emitted within most grains due to their small size. The dislocations that are emitted move freely across the larger grains to the surface, where they annihilate. Lattice rotations seem to effectively lower the internal energy in our system already.
- Differential EBSD tomography was introduced as a powerful tool to detect and elucidate even slight microstructural changes as well as the differences between various loading conditions.

As outlook, larger non-nanocrystalline systems are currently studied to further observe the behavior of dislocations in case of larger grains as mediators for plasticity. Additionally, the geometry and crystal lattice of the abrasives is being optimized to better resemble alumina abrasives that cut into the work piece more than they plow. Finally, it would be interesting to analyze the residual stresses after the grinding process in a more detailed way to better link the microstructural changes to the actual stress situation in the work piece.

Supplementary data to this article can be found online at https://doi.org/10.1016/j.matdes.2020.109053.

## Data availability

The data supporting the findings of this study are available from the corresponding author upon reasonable request.

## Declaration of Competing Interest

The authors declare that they have no known competing financial interests or personal relationships that could have appeared to influence the work reported in this paper.

## References

[1] P.J. Arrazola, T. Özel, D. Umbrello, M. Davies, I.S. Jawahir, Recent advances in modelling of metal machining processes, CIRP Ann. 62 (2) (2013) 695–718.

[2] I.S. Jawahir, E. Brinksmeier, R. M'saoubi, D.K. Aspinwall, J.C. Outeiro, D. Meyer, D. Umbrello, A.D. Jayal, Surface integrity in material removal processes: recent advances, CIRP Ann. 60 (2) (2011) 603–626.

[3] Hao Nan Li, Tian Biao Yu, Li Da Zhu, Wan Shan Wang, Analytical modeling of grinding-induced subsurface damage in monocrystalline silicon, Mater. Design 130 (2017) 250–262.

[4] Kenneth Holmberg, Allan Matthews, Coatings Tribology: Properties, Mechanisms, Techniques and Applications in Surface Engineering, Elsevier, 2009.

[5] Fehim Findik, Latest progress on tribological properties of industrial materials, Mater. Des. 57 (2014) 218–244.

[6] Christian Greiner, Johanna Gagel, Peter Gumbsch, Solids under extreme shear: Friction-mediated subsurface structural transformations, Adv. Mater. 31 (26) (2019) 1806705.

[7] Philipp G. Grützmacher, Sebastian Rammacher, Dominic Rathmann, Christian Motz, Frank Mücklich, Sebastian Suarez, Interplay between microstructural evolution and tribo-chemistry during dry sliding of metals, Friction 7 (6) (2019) 637–650.

[8] Nicolas Argibay, M. Chandross, Shengfeng Cheng, Joseph R. Michael, Linking microstructural evolution and macro-scale friction behavior in metals, J. Mater. Sci. 52 (5) (2017) 2780–2799.

[9] A. Mahyar Khorasani, M. Reza Soleymani Yazdi, Mir Saeed Safizadeh, Analysis of machining parameters effects on surface roughness: a review, Int. J. Comput. Mater. Sci. Surface Eng. 5 (1) (2012) 68–84.

[10] Fukuo Hashimoto, Hitomi Yamaguchi, Peter Krajnik, Konrad Wegener, Rahul Chaudhari, Hans-Werner Hoffmeister, Friedrich Kuster, Abrasive fine-finishing technology, CIRP Ann. 65 (2) (2016) 597–620.

[11] S. Satorres Martnez, C. Ortega Vázquez, J. Gámez Garca, J. Gómez Ortega, Quality inspection of machined metal parts using an image fusion technique, Measurement 111 (2017) 374–383.

[12] Thomas Spenger, Franz Haas, Ulrike Cihak-Bayr, Stefan J. Eder, Markus Weiß, Martin Weinzerl, Michael Schneider, RPM-synchronous grinding — investigation and comparison of surface topography of Synchro-Finish manufactured workpieces, Procedia CIRP 81 (2019) 476–481.

[13] M.R.H. Mohd, Adnan, Arezoo Sarkheyli, Azlan Mohd Zain, and Habibollah Haron. Fuzzy logic for modeling machining process: a review, Artif. Intell. Rev. 43 (3) (2015) 345–379.

[14] S.G. Acharyya, A. Khandelwal, V. Kain, A. Kumar, I. Samajdar, Surface working of 304l stainless steel: impact on microstructure, electrochemical behavior and scc resistance, Mater. Charact. 72 (2012) 68–76.

[15] S. Tarasov, V. Rubtsov, A. Kolubaev, Subsurface shear instability and nanostructuring of metals in sliding, Wear 268 (1) (2010) 59–66.

[16] J.F. Belak, I.F. Stowers, A molecular dynamics model of the orthogonal cutting process, Technical report, Lawrence Livermore National Lab., CA (USA), 1990.

[17] Liangchi Zhang, Hiroaki Tanaka, Towards a deeper understanding of wear and friction on the atomic scale–a molecular dynamics analysis, Wear 211 (1) (1997) 44–53.

[18] R. Komanduri, N. Chandrasekaran, L.M. Raff, MD simulation of indentation and scratching of single crystal aluminum, Wear 240 (1–2) (2000) 113–143.

[19] A. Hasnaoui, H. Van Swygenhoven, P.M. Derlet, Cooperative processes during plastic deformation in nanocrystalline fcc metals: a molecular dynamics simulation, Phys. Rev. B 66 (18) (2002) 184112.

[20] H. Van Swygenhoven, P.M. Derlet, A.G. Frøseth, Stacking fault energies and slip in nanocrystalline metals, Nat. Mater. 3 (6) (2004) 399–403.

[21] V. Yamakov, D. Wolf, S.R. Phillpot, A.K. Mukherjee, H. Gleiter, Deformation-mechanism map for nanocrystalline metals by molecular-dynamics simulation, Nat. Mater. 3 (1) (2004) 43–47.

[22] M. Rajagopalan, K. Darling, S. Turnage, R.K. Koju, B. Hornbuckle, Y. Mishin, K.N. Solanki, Microstructural evolution in a nanocrystalline Cu-Ta alloy: a combined in-situ TEM and atomistic study, Mater. Des. 113 (2017) 178–185.

[23] Ellad B. Tadmor, Ronald E. Miller, Modeling materials: continuum, atomistic and multiscale techniques, Cambridge University Press, 2011.

[24] E. Badisch, M. Varga, S.J. Eder, A brief review of abrasive wear modelling using a numerical-experimental approach, Key Engineering Materials, 799, Trans Tech Publ 2019, pp. 83–88.

[25] Angelos P. Markopoulos, Nikolaos E. Karkalos, Emmanouil-Lazaros Papazoglou, Meshless methods for the simulation of machining and micro-machining: a review, Arch. Comput. Methods Eng. 27 (3) (2020) 831–853.

[26] S.J. Eder, M. Rodrguez Ripoll, U. Cihak-Bayr, D. Dini, C. Gachot, Unraveling and mapping the mechanisms for near-surface microstructure evolution in CuNi alloys under sliding, ACS Appl. Mater. Interfaces 12 (28) (2020) 32197–32208.

[27] Pedro A. Romero, Tommi T. Järvi, Nils Beckmann, Matous Mrovec, Michael Moseler, Coarse graining and localized plasticity between sliding nanocrystalline metals, Phys. Rev. Lett. 113 (3) (2014), 036101.

[28] Ao Li, Izabela Szlufarska, How grain size controls friction and wear in nanocrystalline metals, Phys. Rev. B 92 (7) (2015) 075418.

[29] C. Kale, S. Turnage, P. Garg, I. Adlakha, S. Srinivasan, B.C. Hornbuckle, K. Darling, K.N. Solanki, Thermo-mechanical strengthening mechanisms in a stable nanocrystalline binary alloy – a combined experimental and modeling study, Mater. Des. 163 (2019) 107551.

[30] S.J. Eder, U. Cihak-Bayr, D. Bianchi, Single-asperity contributions to multi-asperity wear simulated with molecular dynamics, IOP Conference Series: Materials Science and Engineering 119 (1) (2016) 012009.

[31] Christian Greiner, Zhilong Liu, Reinhard Schneider, Lars Pastewka, Peter Gumbsch, The origin of surface microstructure evolution in sliding friction, Scr. Mater. 153 (2018) 63–67.

[32] Tevis D.B. Jacobs, Christian Greiner, Kathryn J. Wahl, Robert W. Carpick, Insights into tribology from in situ nanoscale experiments, MRS Bull. 44 (6) (2019) 478–486.

[33] S.J. Eder, U. Cihak-Bayr, C. Gachot, M Rodríguez Ripoll, Interfacial microstructure evolution due to strain path changes in sliding contacts, ACS Appl. Mater. Interfaces 10 (28) (2018) 24288–24301.

[34] Saurav Goel, Xichun Luo, Anupam Agrawal, Robert L. Reuben, Diamond machining of silicon: a review of advances in molecular dynamics simulation, International Journal of Machine Tools and Manufacture 88 (2015) 131–164.

[35] S.J. Eder, U. Cihak-Bayr, D. Bianchi, Large-scale molecular dynamics simulations of nanomachining, Adv. Mach. Process. Innov. Model. Tech. 141 (2017).

[36] K.S. Kumar, H. Van Swygenhoven, S. Suresh, Mechanical behavior of nanocrystalline metals and alloys, Acta Mater. 51 (19) (2003) 5743–5774.

[37] Eric Gaffet, Gérard Le Caër, Mechanical processing for nanomaterials, Encyclopedia of Nanoscience and Nanotechnology, 5, American Scientific Publishers Stevenson Ranch, Calif, USA 2004, pp. 91–129.

[38] S.J. Plimpton, Fast parallel algorithms for short-range molecular dynamics, J. Comput. Phys. 117 (1995) 1–19.

[39] S.J. Eder, D. Bianchi, U. Cihak-Bayr, K. Gkagkas, Methods for atomistic abrasion simulations of laterally periodic polycrystalline substrates with fractal surfaces, Comput. Phys. Commun. 212 (2017) 100–112.

[40] M.I. Mendelev, S. Han, D.J. Srolovitz, G.J. Ackland, D.Y. Sun, M. Asta, Development of new interatomic potentials appropriate for crystalline and liquid iron, Philos. Mag. 83 (December 2003) 3977–3994.

[41] S.J. Eder, U. Cihak-Bayr, A. Vernes, G. Betz, Evolution of topography and material removal during nanoscale grinding, J. Phys. D. Appl. Phys. 48 (2015) 465308.

[42] K. Maekawa, A. Itoh, Friction and tool wear in nano-scale machining—a molecular dynamics approach, Wear 188 (1) (1995) 115–122.

[43] Q.X. Pei, C. Lu, H.P. Lee, Y.W. Zhang, Study of materials deformation in nanometric cutting by large-scale molecular dynamics simulations, Nanoscale Res. Lett. 4 (5) (2009) 444–451.

[44] Joachim Mayer, Robert Engelhorn, Rosemarie Bot, Thomas Weirich, Cleo Herwartz, Fritz Klocke, Wear characteristics of second-phase-reinforced sol–gel corundum abrasives, Acta Mater. 54 (13) (2006) 3605–3615.

[45] Leire Godino, Iñigo Pombo, Jose Antonio Sanchez, and Borja Izquierdo. An original tribometer to analyze the behavior of abrasive grains in the grinding process, Metals 8 (7) (2018) 557.

[46] A. Caro, M. Victoria, Ion-electron interaction in molecular-dynamics cascades, Phys. Rev. A 40 (5) (1989) 2287.

[47] Q. Hou, M. Hou, L. Bardotti, B. Prével, P. Mélinon, A. Perez, Deposition of $Au^N$ clusters on Au (111) surfaces. I. Atomic-scale modeling, Phys. Rev. B 62 (4) (2000) 2825.

[48] S.J. Eder, U. Cihak-Bayr, D. Bianchi, G. Feldbauer, G. Betz, Thermostat influence on the structural development and material removal during abrasion of nanocrystalline ferrite, ACS Appl. Mater. Interfaces 9 (15) (2017) 13713–13725.

[49] Y.S. Touloukian, R.W. Powell, C.Y. Ho, P.G. Klemens, Thermophysical Properties of Matter – the TPRC Data Series. Volume 1. Thermal Conductivity – Metallic Elements and Alloys, 1970.

[50] Peter Mahler Larsen, Søren Schmidt, Jakob Schiøtz, Robust structural identification via polyhedral template matching, Modell. Simul. Mater. Sci. Eng. 24 (5) (2016) 055007.

[51] Alexander Stukowski, Visualization and analysis of atomistic simulation data with OVITO–the open visualization tool, Modell. Simul. Mater. Sci. Eng. 18 (1) (2009) 015012.

[52] F. Bachmann, Ralf Hielscher, Helmut Schaeben, Texture analysis with MTEX–free and open source software toolbox, Solid State Phenom., 160, Trans Tech Publ 2010, pp. 63–68.

[53] Gert Nolze, R. Hielscher, Orientations–perfectly colored, J. Appl. Crystallogr. 49 (5) (2016) 1786–1802.

[54] Y.B. Wang, B.Q. Li, M.L. Sui, S.X. Mao, Deformation-induced grain rotation and growth in nanocrystalline ni, Appl. Phys. Lett. 92 (1) (2008), 011903.

[55] Zhiliang Pan, Timothy J. Rupert, Mechanisms of near-surface structural evolution in nanocrystalline materials during sliding contact, Phys. Rev. Mater. 1 (4) (2017) 043602.

[56] N. Argibay, T.A. Furnish, B.L. Boyce, B.G. Clark, M. Chandross, Stress-dependent grain size evolution of nanocrystalline ni-w and its impact on friction behavior, Scr. Mater. 123 (2016) 26–29.

[57] M. Jin, A.M. Minor, E.A. Stach, J.W. Morris Jr., Direct observation of deformation-induced grain growth during the nanoindentation of ultrafine-grained al at room temperature, Acta Mater. 52 (18) (2004) 5381–5387.

[58] Timothy J. Rupert, Christopher A. Schuh, Sliding wear of nanocrystalline ni–w: structural evolution and the apparent breakdown of archard scaling, Acta Mater. 58 (12) (2010) 4137–4148.

[59] A. Kazemi Talachi, M. Eizadjou, H. Danesh Manesh, K. Janghorban, Wear characteristics of severely deformed aluminum sheets by accumulative roll bonding (arb) process, Mater. Charact. 62 (1) (2011) 12–21.

[60] Shan Zhiwei, E.A. Stach, J.M.K. Wiezorek, J.A. Knapp, D.M. Follstaedt, S.X. Mao, Grain boundary-mediated plasticity in nanocrystalline nickel, Science 305 (5684) (2004) 654–657.

[61] Bin Chen, Katie Lutker, Jialin Lei, Jinyuan Yan, Shizhong Yang, Ho-kwang Mao, Detecting grain rotation at the nanoscale, Proc. Natl. Acad. Sci. 111 (9) (2014) 3350–3353.

[62] N.Q. Vo, Robert S. Averback, Pascal Bellon, S. Odunuga, A. Caro, Quantitative description of plastic deformation in nanocrystalline cu: dislocation glide versus grain boundary sliding, Phys. Rev. B 77 (13) (2008) 134108.

[63] Zoheir N. Farhat, Contribution of crystallographic texturing to the sliding friction behaviour of fcc and hcp metals, Wear 250 (1–12) (2001) 401–408.

[64] Alexander Stukowski, Vasily V. Bulatov, Athanasios Arsenlis, Automated identification and indexing of dislocations in crystal interfaces, Modell. Simul. Mater. Sci. Eng. 20 (8) (2012) 085007.

[65] Tetsuya Ohashi, Masato Kawamukai, Hussein Zbib, A multiscale approach for modeling scale-dependent yield stress in polycrystalline metals, Int. J. Plast. 23 (5) (2007) 897–914.

[66] Liu Chen, Fuping Yuan, Ping Jiang, Jijia Xie, Xiaolei Wu, Mechanical properties and deformation mechanism of mg-al-zn alloy with gradient microstructure in grain size and orientation, Mater. Sci. Eng. A 694 (2017) 98–109.

[67] M. Zhao, J.C. Li, Q. Jiang, Hall–petch relationship in nanometer size range, J. Alloys Compd. 361 (1–2) (2003) 160–164.

[68] Jong Bae Jeon, Byeong-Joo Lee, Young Won Chang, Molecular dynamics simulation study of the effect of grain size on the deformation behavior of nanocrystalline body-centered cubic iron, Scr. Mater. 64 (6) (2011) 494–497.

[69] Carsten Gachot, Philipp Grützmacher, Andreas Rosenkranz, Laser surface texturing of tial multilayer films—effects of microstructure and topography on friction and wear, Lubricants 6 (2) (2018) 36.